Gait analysis using gravitational acceleration measured by wearable sensors

Ryo Takeda [a], Shigeru Tadano [a*], Masahiro Todoh [a]

Manabu Morikawa [b], Minoru Nakayasu [c], Satoshi Yoshinari [d]

[a] Division of Human Mechanical Systems and Design, Graduate School of Engineering, Hokkaido University, Sapporo, Japan

[b] Formerly Division of Human Mechanical Systems and Design, Graduate School of Engineering, Hokkaido University, Sapporo, Japan (Currently at Kawasaki Heavy Industries, Ltd)

[c] Formerly Division of Human Mechanical Systems and Design, Graduate School of Engineering, Hokkaido University, Sapporo, Japan (Currently at Denso Corporation)

[d] Human Engineering Section, Product Technology Department, Hokkaido Industrial Research Institute, Sapporo, Japan

* Corresponding Author:

Shigeru TADANO, PhD

Professor, Division of Human Mechanical Systems and Design, Graduate School of Engineering, Hokkaido University

N13 W8, Kita-ku, Sapporo 060-8628, Japan

Tel/Fax: +81-11-706-6405, E-mail: tadano@eng.hokudai.ac.jp

Keywords: Gait Analysis; Acceleration Sensor; Gravitational Acceleration; Frequency Analysis

Word count: 2987 words (Introduction through Acknowledgment)

Manuscript Type: Original Article

Abstract

A novel method for measuring human gait posture using wearable sensor units is proposed. The sensor units consist of a tri-axial acceleration sensor and three gyro sensors aligned on three axes. The acceleration and angular velocity during walking were measured with seven sensor units worn on the abdomen and the lower limb segments (both thighs, shanks and feet). The three dimensional positions of each joint are calculated from each segment length and joint angle. Joint angle can be estimated mechanically from the gravitational acceleration along the anterior axis of the segment. However, the acceleration data during walking includes three major components; translational acceleration, gravitational acceleration and external noise. Therefore, an optimization analysis was represented to separate only the gravitational acceleration from the acceleration data. Because the cyclic patterns of acceleration data can be found during constant walking, a FFT analysis was applied to obtain some characteristic frequencies in it. A pattern of gravitational acceleration was assumed using some parts of these characteristic frequencies. Every joint position was calculated from the pattern under the condition of physiological motion range of each joint. An optimized pattern of the gravitational acceleration was selected as a solution of an inverse problem. Gaits of three healthy volunteers were measured by walking for 20 seconds on a flat floor. As a result, the acceleration data of every segment was measured simultaneously. The characteristic three-dimensional walking could be shown by the expression using a stick figure model. In addition, the trajectories of the knee joint in the horizontal plane could be checked by visual imaging on a PC. Therefore, this method provides important quantitive information for gait diagnosis.

1. Introduction

Currently, the main method for gait analysis is done by tracking a patient's movement through camera systems, like the Vicon motion analysis system (Vicon Motion Systems, Inc.). These systems can provide three-dimensional position of body segments, but use of these systems is generally indoors in laboratories.

An alternate method for monitoring human motion proposed by Morris, suggested that acceleration sensors fixed on the body could be used to identify human movement (Morris, 1973). Wearable sensor systems have advantages over camera based systems because measurements can be conducted outside the laboratories to monitor daily human activities (Veltink et al., 1996; Bouten et al., 1997; Bussmann et al., 1998; Foerster et al., 1999).

However, compared to camera systems wearable sensors systems can not provide position data, but only information such as the tilt angle of a body segment. Therefore, many works in the past using wearable sensors have been limited to monitoring gait events (Jasiewicz et al., 2006; Lau and Tong, 2008) or just comparing acceleration data (Kavanagh et al., 2005).

Some works in the past have investigated using acceleration sensors for obtaining body segment posture and orientation. Luinge created a Kalman filter to separate the gravity vector to obtain inclination angle of an acceleration sensor during crate lifting motion (Luinge, 2002). They succeeded in lowering inclination errors, but errors increased according to speed. Giansanti et al. conducted simulations with acceleration sensors and reported the inclination and position errors for various motions (Giansanti et al., 2003). In all motions error accumulated according to time. They concluded that the acceleration sensors were not suited for long term measurements.

Because of this some works have used a combination of acceleration and gyro sensors. The displacement of acceleration and gyro sensors on the thigh and shank were used to estimate three-dimensional knee joint angles during walking (Dejnabadi et al. 2006; Favre et al., 2008). However these methods were limited to only the knee joint and absolute displacement was not considered. Others have used also used magnetic sensors (Zhu and Zhou, 2004). They used body segment position and orientation calculated by the magnetic sensors to compensate errors calculated by gyro and acceleration sensors. High correlation with camera system was reported, but magnetic sensors are affected by ferrous materials which restrict usage in surroundings with high magnetic interference. This problem was overcome by attaching a magnetic source to the body, removing surrounding magnetic interference (Roetenberg et al., 2007).

Instead of using exterior transmitting sources, such as cameras or magnetic fields, this method used acceleration data to measure tilt angle of lower body segments and gyro sensors to measure abdomen rotation in the horizontal plane. Though, elsewhere (Luinge, 2002; Giansanti et al., 2003) reported difficulties in using acceleration sensors to measure inclination, this work propose to an alternate method for calculating lower limb posture. This work used the cyclic patterns during constant walking to divide the of acceleration data into decomposition patterns. An optimization algorithm, based on physiological motion range of each joint was applied to the patterns. The pattern that presented the lowest amount of position error was considered as the gravitational acceleration. Gaits of three healthy volunteers were measured and the acceleration data of every lower limb segment was measured simultaneously. As a result, three-dimensional walking established in this method could be visualized by using a stick figure model in a base coordinate system.

2. Method

2.1 Model description

Figure 1 depicts the model and coordinate systems used to calculate lower limb human posture during gait. The sensors are placed on seven locations: abdomen, left and right thigh, left and right shank, left and right foot.

2.2 Three-dimensional gait posture calculations

2.2.1 Body segment tilt angle

The three-dimensional position of joints can be calculated from tilt angle and length of each body segment. Segment length is measured from body measurements and tilt angle of a segment is equal to the tilt angle of the attached acceleration sensor. The tilt angle θ_{XZ}^{α}, of segment α, is calculated using the measured acceleration a_x^{α} and gravitational acceleration g.

$$\theta_{XZ}^{\alpha} = sin^{-1}\left(\frac{a_x^{\alpha}}{g}\right) \tag{1}$$

Here, a_x^{α} is the gravitational acceleration measured in the x^{α} axis direction. The gravitational acceleration is constant but the gravitational acceleration measured in the x^{α} axis of the acceleration sensors varies according to tilt angle of segment. Gyro sensors are used to measure the horizontal rotation of the abdomen during gait. Rotation angle θ_{XY}^{AB} is calculated by integrating angular velocity ω_{XY}, measured from the gyro sensor placed on the abdomen.

$$\theta_{XY}^{AB} = \int \omega_{XY} dt \tag{2}$$

Integrating raw angular velocity data will result in drift error, therefore a high-pass filter is applied to the angular velocity data to remove noise before integration.

2.2.2 Frequency analysis

Acceleration data collected by the acceleration sensors during motion has three major components: translational acceleration, gravitational acceleration, and external noise (Luinge et al., 1999). Therefore a method to separate the gravitational acceleration was developed.

First the acceleration data measured by the acceleration sensor is processed to remove noise (Fig. 2). During constant walking cyclic patterns in the acceleration data can be observed. Previously, similar cyclic patterns have been reported in the movement of body segments during constant walking (Grossman et al., 1988; Lamoth et al., 2002). Fast Fourier transformation is applied to the acceleration data for frequency analysis and peaks at certain frequencies were found (Fig. 2(b)). The first frequency peak is the same frequency as the walking frequency and defined as the primary GF (gait frequency). Other peaks appeared at frequencies multiple of the primary GF. The data of these frequencies includes both the gravitational acceleration and the translational acceleration.

This work focuses on the first three low frequencies in Fig. 2(b), the primary GF, secondary GF, and tertiary GF. The acceleration data of the primary, secondary, and tertiary GFs were extracted using low-pass and band-pass filters (Fig. 2(c)). As shown in Fig. 2(a), the combined data coincides with the original acceleration data with noise removed.

2.2.3 Wave decomposition

Wave decomposition is performed on the secondary and tertiary GF acceleration data (Fig. 3). The acceleration data of the primary GF is $a_P^{\alpha}(t)$, where α

represents body segment, and the pattern for $a_P^{\alpha}(t)$ is defined as P01. Wave decomposition is conducted by dividing the secondary and tertiary GF data into peaks and valleys, with 0 as threshold. The acceleration data for the secondary GF is $a_S^{\alpha}(t)$, and the patterns are defined as S01, S02, S03 and S04. The acceleration data for the tertiary GF is $a_T^{\alpha}(t)$, and the patterns are defined as T01, T02, T03, T04, T05 and T06.

2.2.4 Determination of gravitational acceleration

An optimization algorithm was developed to establish which pattern or which combination of the patterns represents the gravitational acceleration. The gravitational acceleration is defined as $\boldsymbol{a}_g^{\alpha}$ and expressed in Eq. (3):

$$\boldsymbol{a}_g^{\alpha} = \mathbf{C_P}\mathbf{A}_{\mathbf{P}}^{\alpha} + \mathbf{C_S}\mathbf{A}_{\mathbf{S}}^{\alpha} + \mathbf{C_T}\mathbf{A}_{\mathbf{T}}^{\alpha} \tag{3}$$

$$\mathbf{A}_{\mathbf{P}}^{\alpha} = (a_{P01}^{\alpha})^T \tag{4}$$

$$\mathbf{A}_{\mathbf{S}}^{\alpha} = (a_{S01}^{\alpha}, a_{S02}^{\alpha}, a_{S03}^{\alpha}, a_{S04}^{\alpha})^T \tag{5}$$

$$\mathbf{A}_{\mathbf{T}}^{\alpha} = (a_{T01}^{\alpha}, a_{T02}^{\alpha}, a_{T03}^{\alpha}, a_{T04}^{\alpha}, a_{T05}^{\alpha}, a_{T06}^{\alpha})^T \tag{6}$$

Here (4), (5), and (6) represent the patterns for $a_P^{\alpha}(t)$, $a_S^{\alpha}(t)$,and $a_T^{\alpha}(t)$ respectively. The $\mathbf{C_P}$ 1×1 matrix, $\mathbf{C_S}$ 1×4 matrix, and $\mathbf{C_T}$ 1×6 matrix represent combinations of $\mathbf{A}_{\mathbf{P}}^{\alpha}$, $\mathbf{A}_{\mathbf{S}}^{\alpha}$, and $\mathbf{A}_{\mathbf{T}}^{\alpha}$ expressed by 1 or 0. There are 2^4 = 16 patterns for $\mathbf{C_P}$ and 2^6 = 64 patterns for $\mathbf{C_S}$, giving a total of 16 × 64 = 1024 patterns for each sensor. Seven segments mean that the total number of combinations will equal 1024^7. The objective of the optimization algorithm is to determine the optimum $\mathbf{C_P}$, $\mathbf{C_S}$, and $\mathbf{C_T}$ sets.

Searching among 1024^7 combinations is practically difficult so the number of combinations is reduced based on the body segment, as shown in Table 1. Since this work targeted normal walking, it was assumed that the right and left combinations

were bilaterally-symmetric. Ultimately, the total number of combination is limited to 16,777,216 (1024 patterns for the foot × 1024 patterns for the shank × 16 patterns for the thigh).

A combination for the gravitational acceleration was selected as the solution to an inverse problem using the optimization algorithm (Fig. 4). First, one combination pattern is considered as a_x^{α} and the tilt angle of each body segment is calculated using Eq. (1), then the ankle, knee and hip joint positions is calculated from the tilt angle and length of segments.

However, to obtain the position of the joints in the base coordinate system, it is necessary to determine the leg on the ground. Elsewhere it was reported that acceleration data can accurately detect gait events such as the heel contact (Currie et al., 1992; Auvinet et al., 2002; Mansfield and Lyons, 2003). This work used sudden drops in the shank acceleration a_x^{RS}, a_x^{LS} to detect the instance of heel contact and determine the leg on the ground. Afterwards, joint positions are calculated using Eq. (7) and (8).

$$\mathbf{J2} = (D_{12} sin\theta_{XZ}^{\alpha} + J1_X, J1_Y, D_{12} cos\theta_{XZ}^{\alpha} + J1_Z) \tag{7}$$

$$\mathbf{H2} = (D_{hip} sin\theta_{XY}^{AB} + H1_{X,} D_{hip} cos\theta_{XY}^{AB} + H1_Y, H1_Z) \tag{8}$$

In Eq. (7) two joint positions $\mathbf{J_1}$ and $\mathbf{J_2}$ are considered, and the calculations are commenced from the ankle joint of the leg on the ground. For example in Fig. 5(a), **RA** is considered as **J1** and **RK** joint is considered as **J2.** D_{12}, the distance between RA and RK, and tilt angle θ_{XZ}^{α} (α being RS) is used to calculate **J2**. Once **RK** is obtained **RK** becomes the new **J1'** and **RH** as the new **J2'**. The position between the right and left hip joints is obtained using Eq. (8). As shown in Fig. 5(b) the position of $\mathbf{H_2}$, or **LH**, is calculated using the distance between the **RH** and **LH** D_{hip} and the angle

of rotation of the abdomen θ_{XY}^{AB}. The hip joint flexion angles are calculated using θ_{XZ}^{LT}, θ_{XZ}^{RT}, and the ankle flexion joints are calculated using θ_{XZ}^{LF}, θ_{XZ}^{RF}. The knee joint flexion angles are obtained using Eq. (9) and (10).

$$\theta^{LK} = \left|\theta_{XZ}^{LS} - \theta_{XZ}^{LT}\right| \tag{9}$$

$$\theta^{RK} = \left|\theta_{XZ}^{RS} - \theta_{XZ}^{RT}\right| \tag{10}$$

The algorithm checks whether the range of motion determined for each joint is within values of Table 2.

Next, RH_X and LH_X are checked to see if they fell between coordinates RA_X and LA_X during heel contact, using Eq. (11) and (12).

$$LA_X < \left|\frac{LH_X + RH_X}{2}\right| < RA_X \tag{11}$$

$$RA_X < \left|\frac{LH_X + RH_X}{2}\right| < LA_X \tag{12}$$

Applying these conditions, the search program discards patterns that result in inadequate joint positions at heel contact as indicated in Fig. 6. After all patterns are checked, an evaluation is made of the patterns that satisfied the algorithm constraints using Eq. (13).

$$U = \sum_{j=1}^{n} \left(RA_{Z,j}^2 + LA_{Z,j}^2 \right) \tag{13}$$

The pattern that produces the least amount of error for RA_Z and LA_Z at the time of heel contact is considered as the gravitational acceleration pattern. Here 1 to n number of steps are considered, with n is the total number of steps of j. An example of a gravitational acceleration pattern obtained using the search program is shown in Fig. 7. The gravitational acceleration pattern gives the tilt angle of each segment and the

three-dimensional lower limb gait posture is calculated with the length of the segments. A stick figure model is used to visually confirm the lower limb posture.

3. Experiment

This sensor system developed for this investigation consisted of seven sensor units, each containing a data logger and a sensor head. The sensor head has a tri-axial acceleration sensor (H34C, Hitachi Metals, Ltd.) and three gyro sensors (ENC-03M, muRata Manufacturing Co., Ltd.) aligned on three orthogonal axes. The data logger simultaneously records the acceleration and angular velocity data for a maximum of 150 seconds at a sampling rate of 100Hz. One sensor unit weighs 136 g, including battery (90 g), and the size is 50mm × 50mm × 15mm for the data logger and 15mm × 15mm × 15mm for the sensor head. An automated mechanical turntable was used to derive the offset for acceleration and angular velocity data of each sensor unit.

Sensor units were placed on seven segments as shown in Fig. 8. A photo transistor inside the data recorder, and activated by a strong flash, was used to commence the measurement of all seven sensors simultaneously. Reflective markers were placed on the lower body of the volunteers and images (frame rate: 60fps) were captured during the experiment using a digital camera (HDR-SR1, Sony Corp.). The camera images were analyzed using motion capture software (DIPP-Motion Pro, Ditect Co., Ltd.). This software automatically detects and gives coordinate data of markers.

Three volunteers, with no past history of disabilities or injuries, participated in this experiment (volunteer information listed in Table 3). Volunteers walked for 20 seconds on a flat straight floor, gait velocity was at the discretion of the volunteers. Measurements for the width at the hip, length of hip joint to knee joint and knee joint to ankle joint were taken for each volunteer. To minimize sensor attachment error, measurements of each sensors unit for each volunteer were measured before and after trials.

4. Results

The anterior axis acceleration data for all seven sensors from one volunteer is shown in Fig. 9. The right leg acceleration of the thigh, shank, and foot are larger than those of the left leg. This could be because the volunteer was right-footed and the right leg showed larger acceleration peaks compared with the left. Hence, this method measures differences in right and left leg acceleration.

Figure 10 shows the frequency analysis of the original anterior axis acceleration data of Fig. 9. It shows that the spectrum for the thigh, shank, and foot are bilaterally-symmetric. The abdomen segment shows that the primary GF was twice that of the other segments. This is because the sensor at the abdomen measures the acceleration of both the right and left leg, thus doubling the frequency.

Figure 11 is a comparison of the calculated hip and knee joint angles with this method and the angles determined using camera images. When looking at the hip joint angle results, there are differences in the 40% to 80% range, but the maximum and minimum peak values are similar. For the knee joint angles, there is consistency between this the results with this system and with the image based system, but peak flexion angle is 10 degrees different.

Figure 12 shows the stick figure representation and knee joint trajectories. This method can visually represent the different walking characteristics of the volunteers.

5. Discussion

The optimization algorithm used for estimating gravitational acceleration was original and created for gait. The advantage of this algorithm is that it gives the optimal lower limb gait posture. This algorithm selects one combination, from 16,777,216 possible combinations, based on joint range of motion and joint positions during heel contact. Other methods such as principle component analysis may find tendencies such as GFs, but separating only the gravitational acceleration is a difficult issue. Our method for selecting the gravitational acceleration is similar to wavelet decomposition, but selecting a predefined wave pattern such as a wavelet coefficient is unnecessary. However, since our algorithm involves searching for a large number of combinations; it may not be suitable for small computing devices.

Though, the algorithm gave optimal lower limb gait posture, joint angles differences were present in Fig. 11. One reason for this could be because, acceleration data are larger at the end segments of the limb, as seen in Fig. 9. Some frequencies containing high amplitude acceleration data at the shank or foot could have been excluded by the low-pass and band-pass filters. These high frequencies could be the reason why differences in the peak flexion angles appeared in the knee but not so much in the hip.

Another reason is in the algorithm itself. Since the estimated gravitational acceleration is the pattern that generated the lowest position error during heel contact, the pattern may not have been the best suited for the swing phase, where the maximum knee flexing occurs. The estimated gravitational acceleration is only a pattern that best fits the constraints during gait, therefore it may not be the true gravitational acceleration. Future works will be to include constraints in the swing

phase of gait and possibly compare gravitational acceleration calculated by camera systems.

In addition, since the gravitational acceleration is estimated using the three GF patterns, the resolution of the joint angles is limited to one third of the primary gait frequency. This could be the reason of phase lags in Fig. 11.

Even with the above considered, the current work showed high differences in joint angles. It may be possible to introduce of gyro sensor measurements to achieve a more accurate estimation of gravitational acceleration. This is still under consideration for future works of this study.

Results presented in this paper showed measurements for gait of healthy volunteers but it would be possible to measure gait of patients with leg disabilities. The right leg acceleration pattern is considered to be the same pattern for the left. Though the same pattern is used, actual acceleration values will vary. Thus, results will show different joint angles. Our method will be able to detect differences in joint angles of a healthy leg and an impaired leg. However, since this method uses FFT for frequency analysis, constant cyclic acceleration data is required. This is why volunteers were asked to walk constant for 20 seconds, meaning analysis for short periods of time will be difficult. Therefore, applying this method will be limited to movement such as walking, running, or ascent and descent of stairs.

Another limitation is that results can not be shown in real time. Work by Kavanagh et al. (Kavanagh et al., 2006) transmitted acceleration data at near real-time speeds via Bluetooth. Though the sensor system presented in this paper cannot provide real-time feedback, we do not consider this as a significant issue compared to results obtained after analysis, such as joint flexion angles and joint position trajectories.

Contrary to limitations, the method described can provide quantitive information for constant gait in healthy subjects, and showed that acceleration patterns during gait can be used to estimate lower body posture.

Acknowledgments

The authors would like to express their thanks to A. Natorigawa of Laboratory of Biomechanical Design (Division of Human Mechanical Systems and Design, Hokkaido University), for her support and cooperation to experiment and computer data analysis of this study.

Conflict of interests

There are no actual or potential conflicts of interest.

References

Auvinet, B., Gloria, E., Renault, G., Barrey, E., 2002. Runner's stride analysis: comparison of kinematic and kinetic analyses under field conditions. Science & Sports, 17, 92-94.

Bouten, C.V.C., Koekkoek, K.T.M., Verduin, M., Kodde, R., Janssen, J.D., 1997. A triaxial accelerometer and portable data processing unit for the assessment of daily physical activity. IEEE Transactions on Biomedical Engineering, 44, 136-147.

Bussmann, J. B. J., van de Laar, Y. M., Neeleman, M. P., Stam, H. J., 1998. Ambulatory accelerometry to quantify motor behaviour in patients after failed back surgery: a validation study. Pain, 74, 153-161.

Currie, G., Rafferty, D., Duncan, G., Bell, F., & Evans, A. L., 1992. Measurement of gait by accelerometer and walkway: a comparison study. Medical and Biological Engineering and Computing, 30, 669-670.

Dejnabadi, H., Jolles, B.M., Casanova, E., Fua, P., Aminian, K., 2006. Estimation and visualization of sagittal kinematics of lower limbs orientation using body-fixed sensors. IEEE Transactions on Biomedical Engineering, 53, 1385-1393.

Favre, J., Jolles, B.M., Aissaoui, R., Aminian, K., 2008. Ambulatory measurement of 3D knee joint angle. Journal of Biomechanics, 41, 1029-1035.

Foerster, F., Smeja, M., Fahrenberg, J., 1999. Detection of posture and motion by accelerometry: a validation study in ambulatory monitoring. Computers in Human Behavior, 15, 571-583.

Giansanti, D., Macellari, V., Maccioni, G., Cappozzo, A., 2003. Is it feasible to reconstruct body segment 3-D position and orientation using accelerometric data?, IEEE Transactions Biomedical Engineering, 50, 476-83

Grossman, G.E., Leigh, R.J., Abel, L.A., Lanska, D.J., Thurston, S.E., 1988. Frequency and velocity of rotational head perturbations during locomotion. Experimental Brain Research, 70, 470-476.

Jasiewicz, J. M., Allum, J. H. J., Middleton, J.W., Barriskill, A., Condie, P., Purcell, B., Li, R. C. T., 2006. Gait event detection using linear accelerometers or angular velocity transducers in able-bodied and spinal-cord injured individuals. Gait & Posture, 24, 502-509.

Kavanagh, J. J., Barrett R. S., Morrison, S., 2005. Age-related differences in head and trunk coordination during walking. Human Movement Science, 24, 574-587.

Lamoth, C.J.C., Beek, P.J., Meijer, O.G., 2002. Pelvis-thorax coordination in the transverse plane during gait, Gait & Posture, 16, 101-114.

Lau, H., Tong, K., 2008. The reliability of using accelerometer and gyroscope for gait event identification on persons with dropped foot, Gait & Posture, 27, 248-257.

Luinge, H. J., Veltink, P.H., Baten, C. T. M., 1999. Estimating orientation with gyroscopes and accelerometers, Technology and Health Care, 7, 455-459.

Luinge, H. J., 2002. Inertial sensing of human movement. PhD. thesis, Twente University Press.

Morris, J.R.W., 1973. Accelerometry - A technique for the measurement of human body movements. Journal of Biomechanics, 6, 729-736.

Mansfield, A., Lyons, G. M., 2003. The use of accelerometry to detect heel contact events for use as a sensor in FES assisted walking, Medical Engineering & Physics, 25, 879-885.

Roetenberg, D.; Slycke, P. J.; Veltink, P. H, 2007. Ambulatory position and orientation tracking fusing magnetic and inertial sensing. IEEE Transactions on Biomedical Engineering, 54, 883-890.

Veltink, P.H., Bussmann, HansB.J., de Vries, W., Martens, WimL.J., Van Lummel, R.C., 1996. Detection of static and dynamic activities using uniaxial accelerometers. IEEE Transactions on Rehabilitation Engineering, 4, 375-385.

Zhu, R., Zhou, Z., 2004. A real-time articulated human motion tracking using tri-axis inertial/magnetic sensors package. IEEE Transactions on Neural Systems and Rehabilitation Engineering, 12, 295-302.

Figure Legends

Figure 1 Gait model and coordinate systems. The *X*, *Y*, *Z* coordinates represents the base coordinate system, where the *X* axis is the walking direction, the *Y* axis is the left-lateral direction, and the *Z* axis is the direction opposite to gravity. The x^{α}, y^{α}, and z^{α} are the measurement coordinate system for segment α (AB, LT, RT, LS, RS, LF and RF), the x^{α} axis is the anterior direction, the y^{α} axis is the left-lateral direction, and the z^{α} axis is the superior direction of the segment.

Figure 2 (a) Original anterior axis acceleration data from x^{LS} (thin line) and combined data of primary, secondary, and tertiary gait frequency (heavy line) during constant walking. (b) Frequency analysis of the original anterior axis acceleration data, and (c) filtered anterior axis acceleration data of the primary, secondary, and tertiary gait frequencies.

Figure 3 Decomposition wave patterns using a single cycle of the primary GF. There are two cycles for the secondary GF and three cycles for the tertiary GF during one primary GF cycle. The secondary GF was divided into two peaks and two valleys, the tertiary GF into three peaks and three valleys, and both used 0 as the threshold.

Figure 4 Flow chart for obtaining an optimal gravitational acceleration pattern.

Figure 5 Joint position calculation method. (a) Calculating the joint positions in the X-Z plane. Right ankle joint is considered as **J1** and right knee joint is considered as **J2**. After **J2** is calculated right knee joint becomes the new **J1'** and right hip joint becomes the new **J2'**. (b) Calculating hip joint positions in X-Y plane.

Figure 6 Adequate and inadequate positions of joint. The gravitational acceleration estimation program eliminated wave patterns that resulted in inadequate joint angle positions during gait, the right hand stick figure here.

Figure 7 Example of estimated gravitational acceleration pattern (P01 + S03 + T01) compared with combined data (primary, secondary, tertiary GF) and original acceleration data.

Figure 8 Sensor unit attachment locations. One sensor unit consisting of a data logger and sensor head is attached on each body segment.

Figure 9 Graphs of the anterior axis acceleration data of all seven sensors. The thin lines represents the original acceleration data of a_x^{AB}, a_x^{LT}, a_x^{RT}, a_x^{LS}, a_x^{RS}, a_x^{LF}, a_x^{RF} and the heavy lines represent the combined data of the primary, secondary, and tertiary GF.

Figure 10 Results of frequency analysis on anterior axis acceleration data using FFT. The vertical axis represents the power spectrum of the acceleration data, and the horizontal axis represents the frequency.

Figure 11 Example of calculated joint angles for volunteers A, B, and C. (1a), (1b), and (1c) are the results for the hip flexion angles. (2a), (2b), and (2c) are the results for knee flexion angles. The thin lines represent the results from the camera based analysis and the heavy lines represent those of the method here. The vertical axis

shows the flexion angle, where 0 is the angle in the upright position, and the horizontal axis shows the percentage of one gait cycle.

Figure 12 Results of the stick figure model created for the three volunteers. (1a) (1b) (1c) are the model for volunteers A, B, and C walking in the X-Z plane. The dark line is the trajectory of the right hip, knee and ankle respectively. (2a) (2b) (2c) are the knee joint trajectory of three volunteers in the horizontal plane.

Table Legend

Table 1 Number of wave patterns used for calculation.

Table 2 Range of motion for each joint.

Table 3 Information of the volunteers. Age, height and the GFs are listed.

Figure1

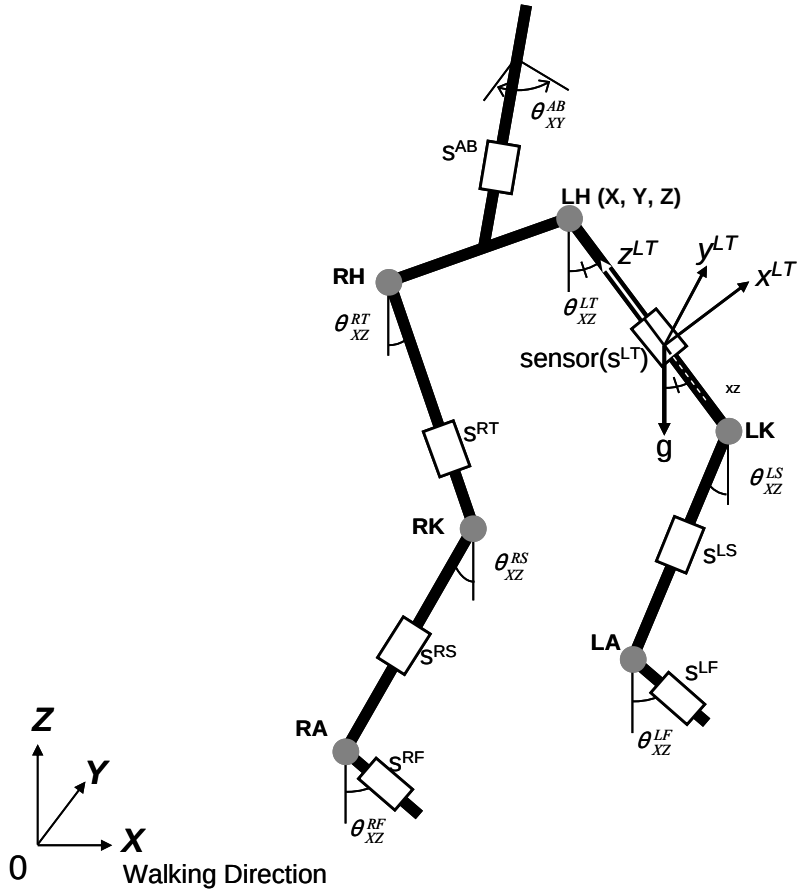

X ,*Y*, *Z* : base coordinate system
X : walking direction, *Y* : lateral direction , *Z*: opposite direction of gravity
x^{α},y^{α} ,z^{α} : measurement coordinate system
θ_{XZ}^{α} : Angle of body segment against gravity direction in *XZ* plane
θ_{XY}^{AB}: Abdomen rotation angle in XY plane

α : *RT* (right thigh), *RS* (right shank), *RF* (right foot),
LT (left thigh), *LS* (left shank), *LF* (left foot), *AB* (abdomen)

Joint Symbols : RH: right hip RK: right knee RA: right ankle
LH: left hip LK: left knee LA: left ankle

Figure2

(a)

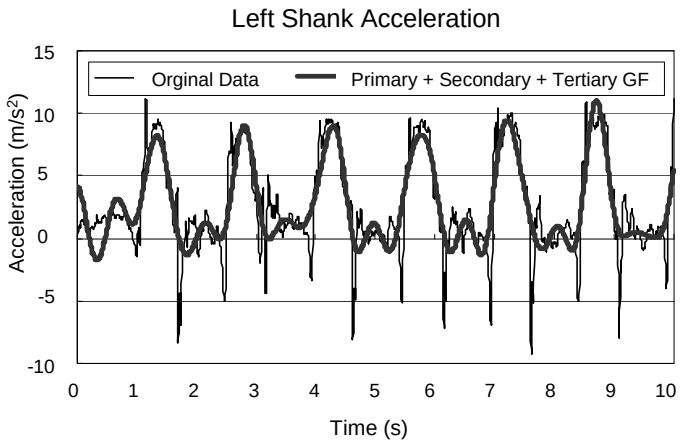
Left Shank Acceleration
Orginal Data
Primary + Secondary + Tertiary GF
Acceleration (m/s2)
15
10
5
0
-5
-10
0
1
2
3
4
5
6
7
8
9
10
Time (s)

(b)

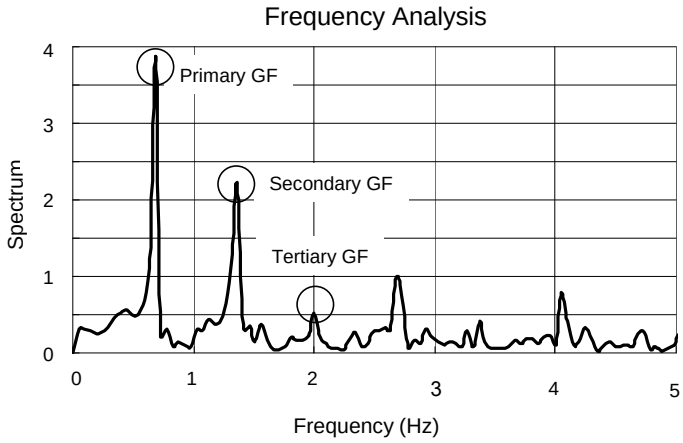
Frequency Analysis
Primary GF
Secondary GF
Tertiary GF
Spectrum
4
3
2
1
0
0
1
2
3
4
5
Frequency (Hz)

(c)

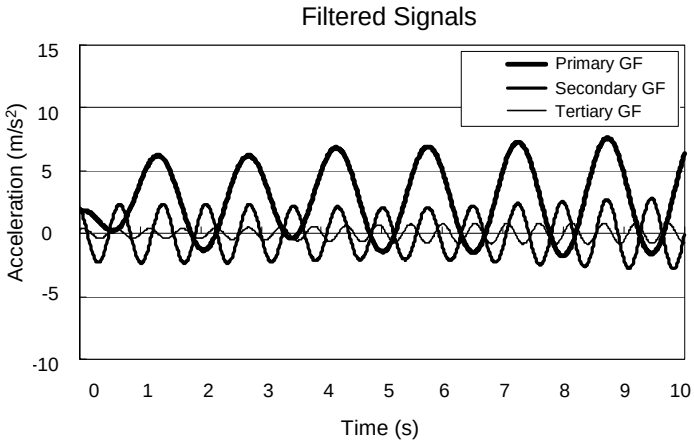
Filtered Signals
Primary GF
Secondary GF
Tertiary GF
Acceleration (m/s2)
15
10
5
0
-5
-10
0
1
2
3
4
5
6
7
8
9
10
Time (s)

Figure 3

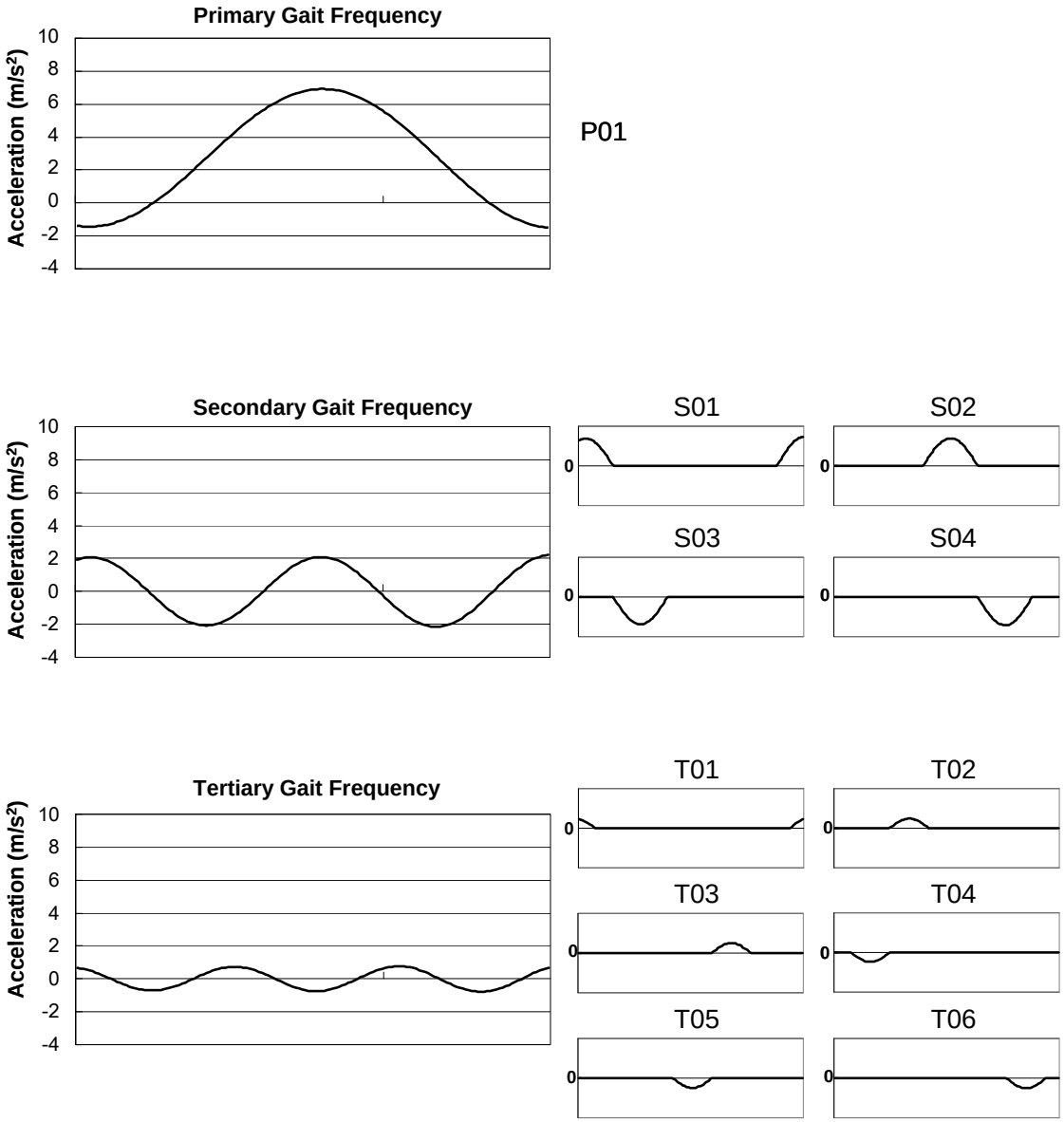
Primary Gait Frequency
Acceleration (m/s²)
10
8
6
4
2
0
-2
-4
P01
Secondary Gait Frequency
Acceleration (m/s²)
S01
S02
S03
S04
0
Tertiary Gait Frequency
Acceleration (m/s²)
T01
T02
T03
T04
T05
T06

Figure 4

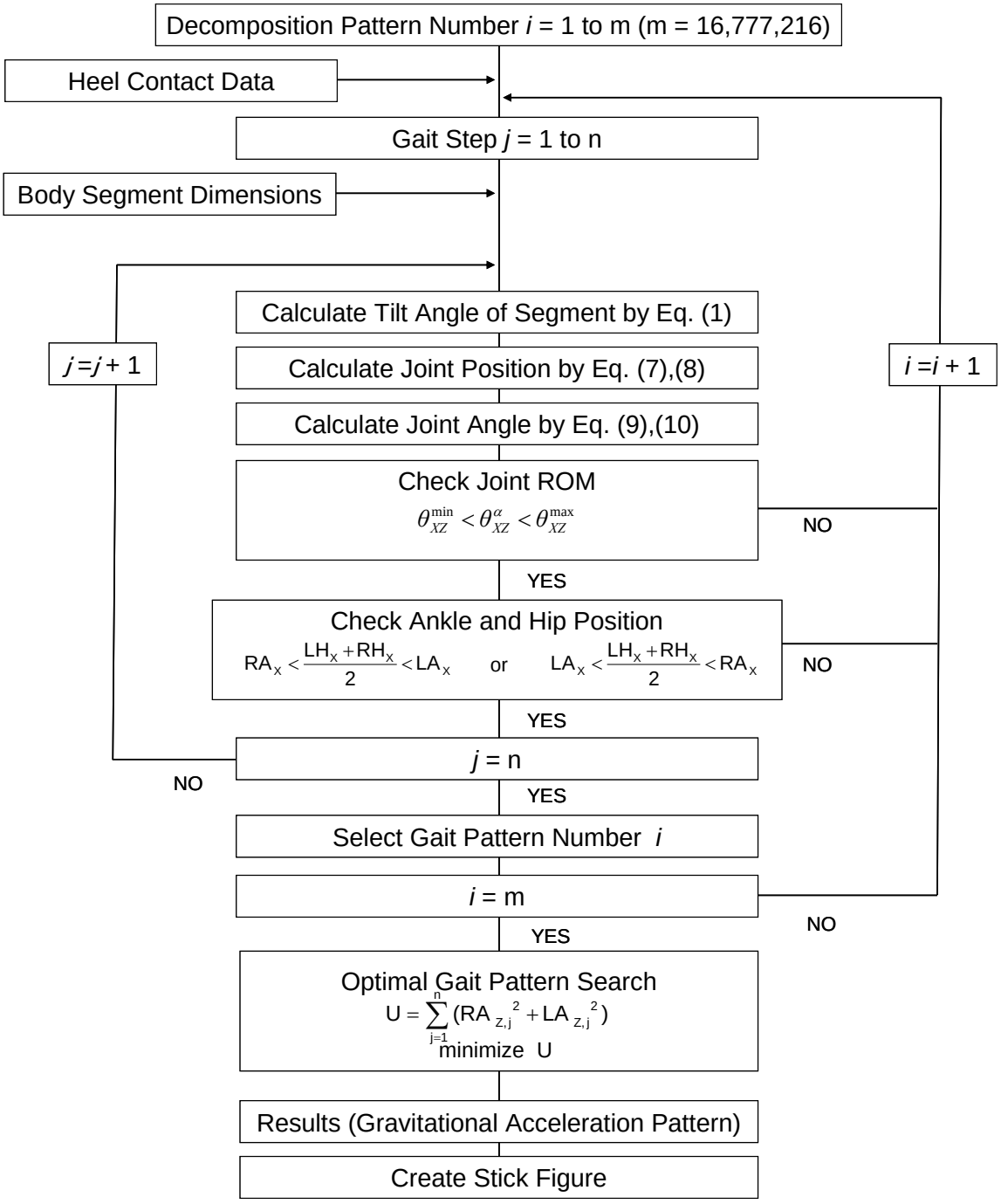
Decomposition Pattern Number i = 1 to m (m = 16,777,216)
Heel Contact Data
Gait Step j = 1 to n
Body Segment Dimensions
Calculate Tilt Angle of Segment by Eq. (1)
j = j + 1
Calculate Joint Position by Eq. (7),(8)
i = i + 1
Calculate Joint Angle by Eq. (9),(10)
Check Joint ROM
$\theta_{XZ}^{\min} < \theta_{XZ}^{\alpha} < \theta_{XZ}^{\max}$
NO
YES
Check Ankle and Hip Position
$RA_X < \frac{LH_X + RH_X}{2} < LA_X$ or $LA_X < \frac{LH_X + RH_X}{2} < RA_X$
NO
YES
j = n
NO
YES
Select Gait Pattern Number i
i = m
NO
YES
Optimal Gait Pattern Search
$U = \sum_{j=1}^{n} (RA_{Z,j}^{2} + LA_{Z,j}^{2})$
minimize U
Results (Gravitational Acceleration Pattern)
Create Stick Figure

Figure 5

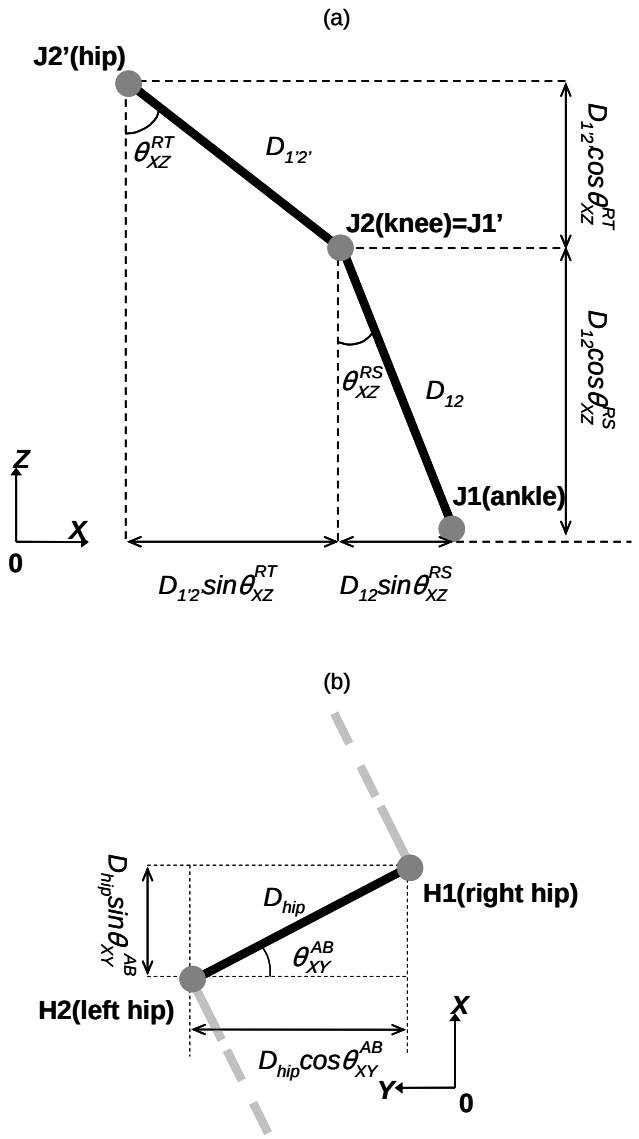
(a)
J2'(hip)
θ_{XZ}^{RT}
$D_{1'2'}$
J2(knee)=J1'
$D_{1'2'}\cos\theta_{XZ}^{RT}$
θ_{XZ}^{RS}
D_{12}
$D_{12}\cos\theta_{XZ}^{RS}$
Z
X
0
J1(ankle)
$D_{1'2'}\sin\theta_{XZ}^{RT}$
$D_{12}\sin\theta_{XZ}^{RS}$
(b)
$D_{hip}\sin\theta_{XY}^{AB}$
D_{hip}
H1(right hip)
θ_{XY}^{AB}
H2(left hip)
X
$D_{hip}\cos\theta_{XY}^{AB}$
Y
0

Figure 6

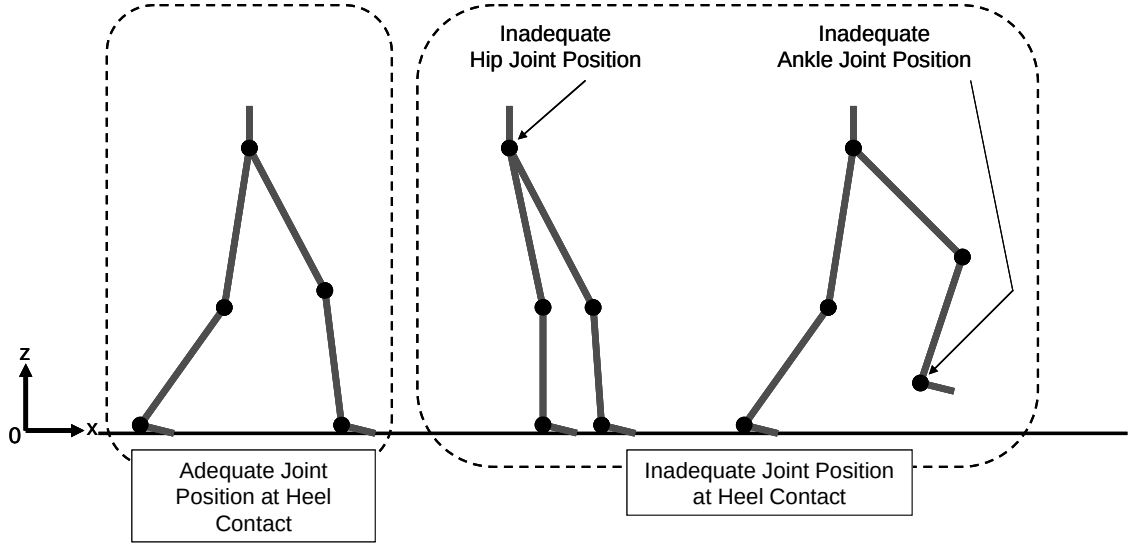
Inadequate
Hip Joint Position
Inadequate
Ankle Joint Position
z
0
x
Adequate Joint
Position at Heel
Contact
Inadequate Joint Position
at Heel Contact

Figure 7

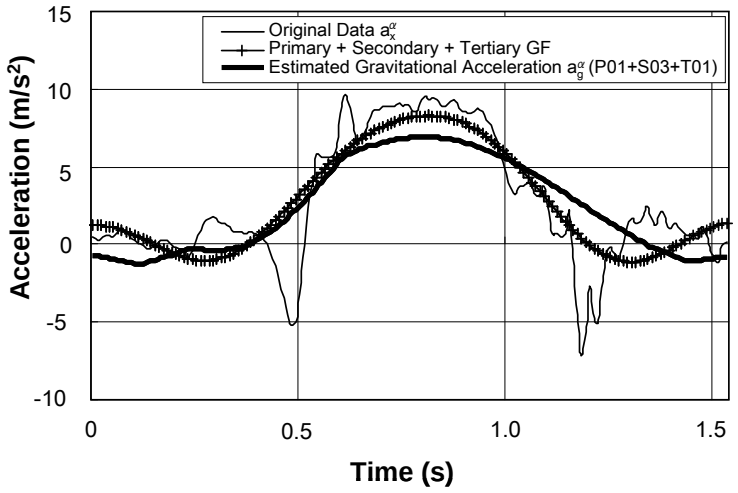
Original Data a_x^α
Primary + Secondary + Tertiary GF
Estimated Gravitational Acceleration a_g^α (P01+S03+T01)
Acceleration (m/s^2)
15
10
5
0
-5
-10
0
0.5
1.0
1.5
Time (s)

Figure 8

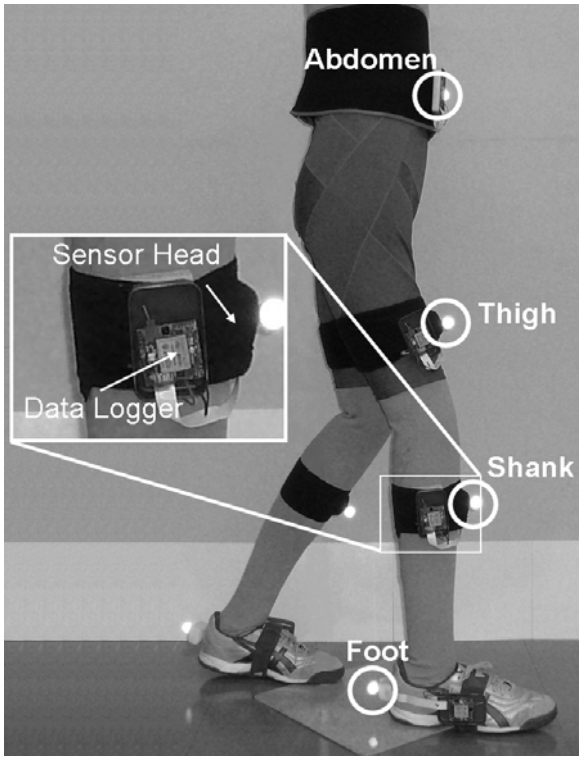

Figure 9

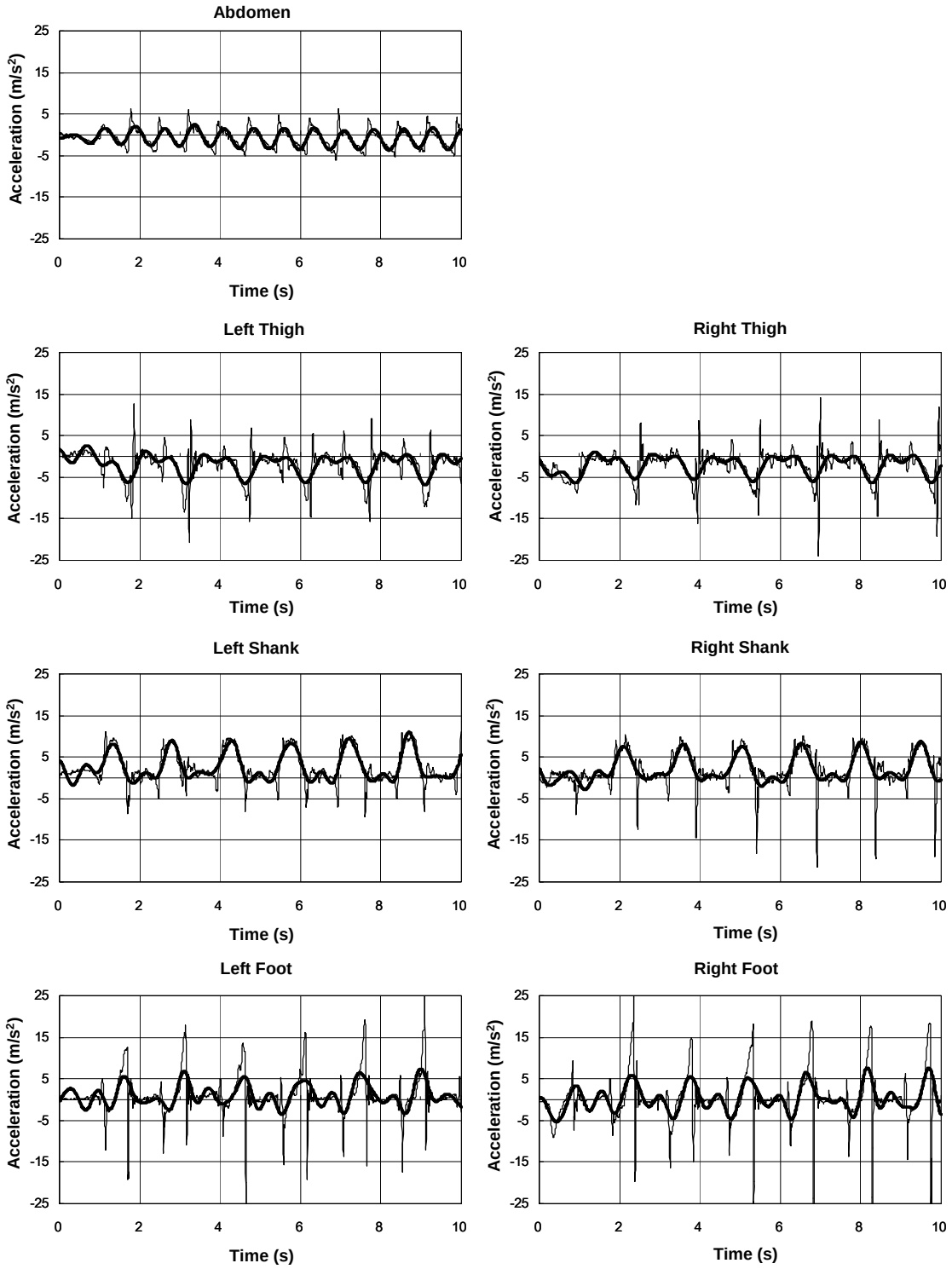
Abdomen
Left Thigh
Right Thigh
Left Shank
Right Shank
Left Foot
Right Foot
Acceleration (m/s²)
Time (s)
25
15
5
-5
-15
-25
0
2
4
6
8
10

Figure 10

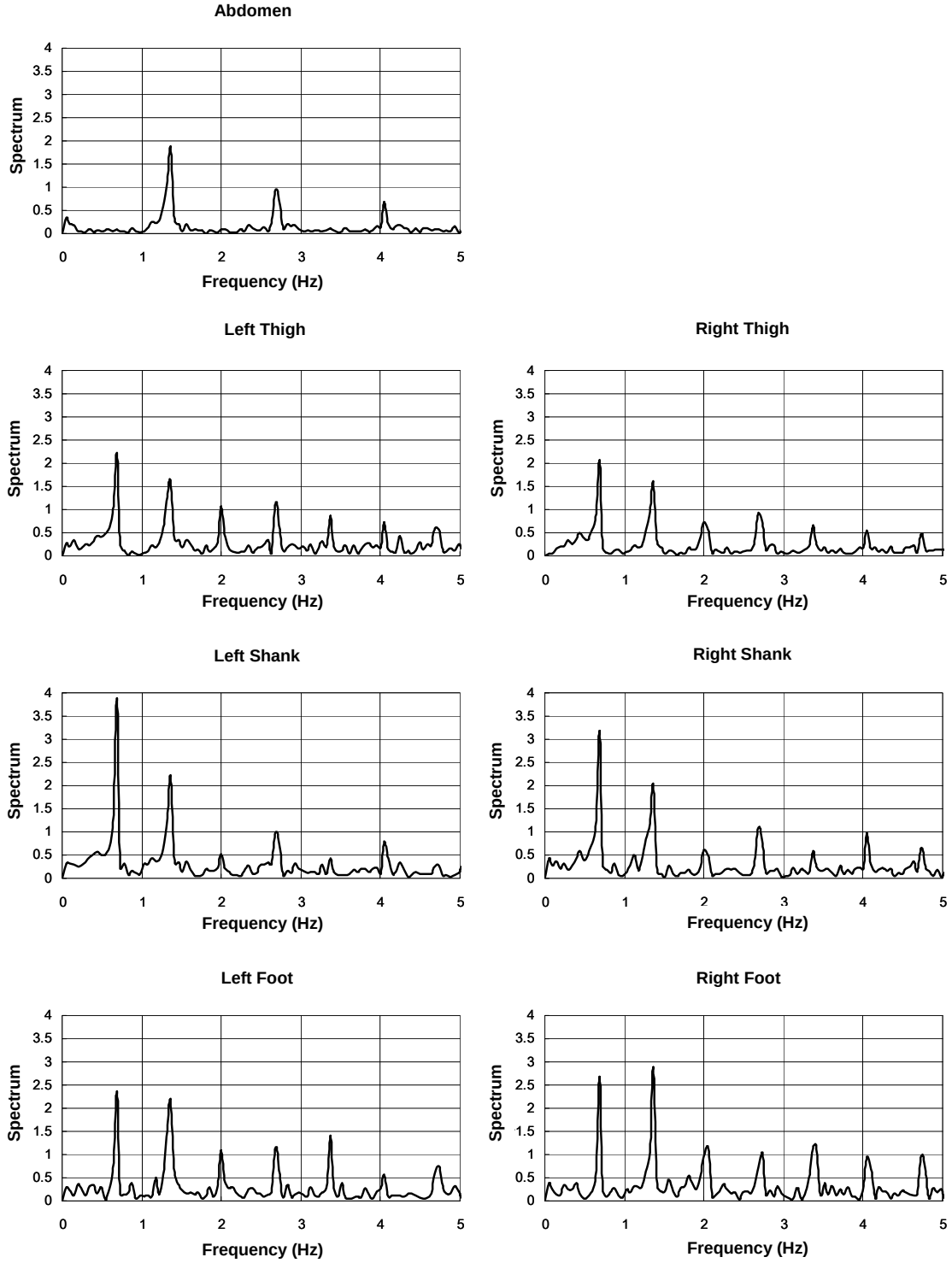
Abdomen
Left Thigh
Right Thigh
Left Shank
Right Shank
Left Foot
Right Foot
Spectrum
Frequency (Hz)
0
0.5
1
1.5
2
2.5
3
3.5
4
5

Figure 11

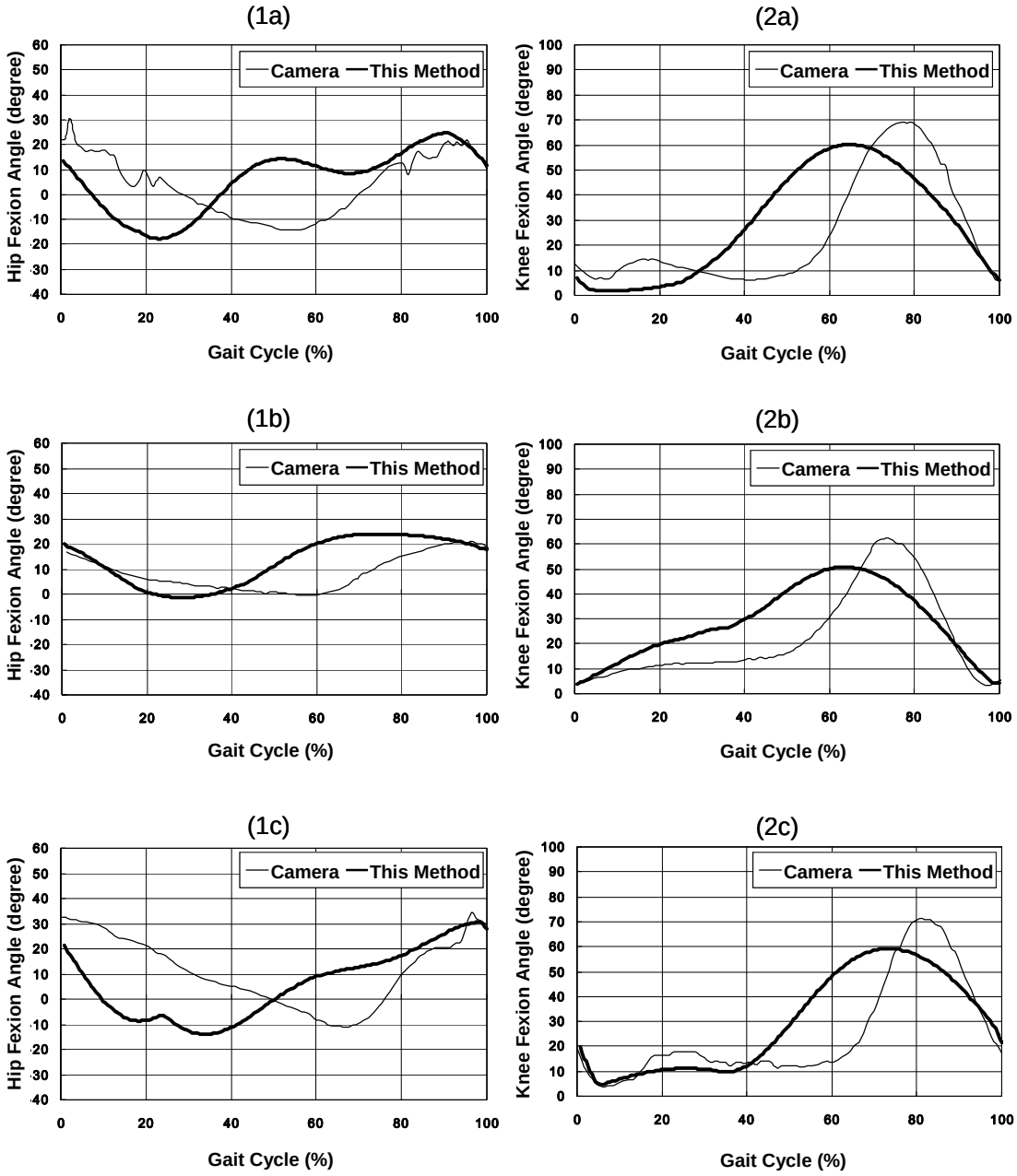
(1a)
(2a)
(1b)
(2b)
(1c)
(2c)
Camera
This Method
Hip Fexion Angle (degree)
Knee Fexion Angle (degree)
Gait Cycle (%)

Figure 12

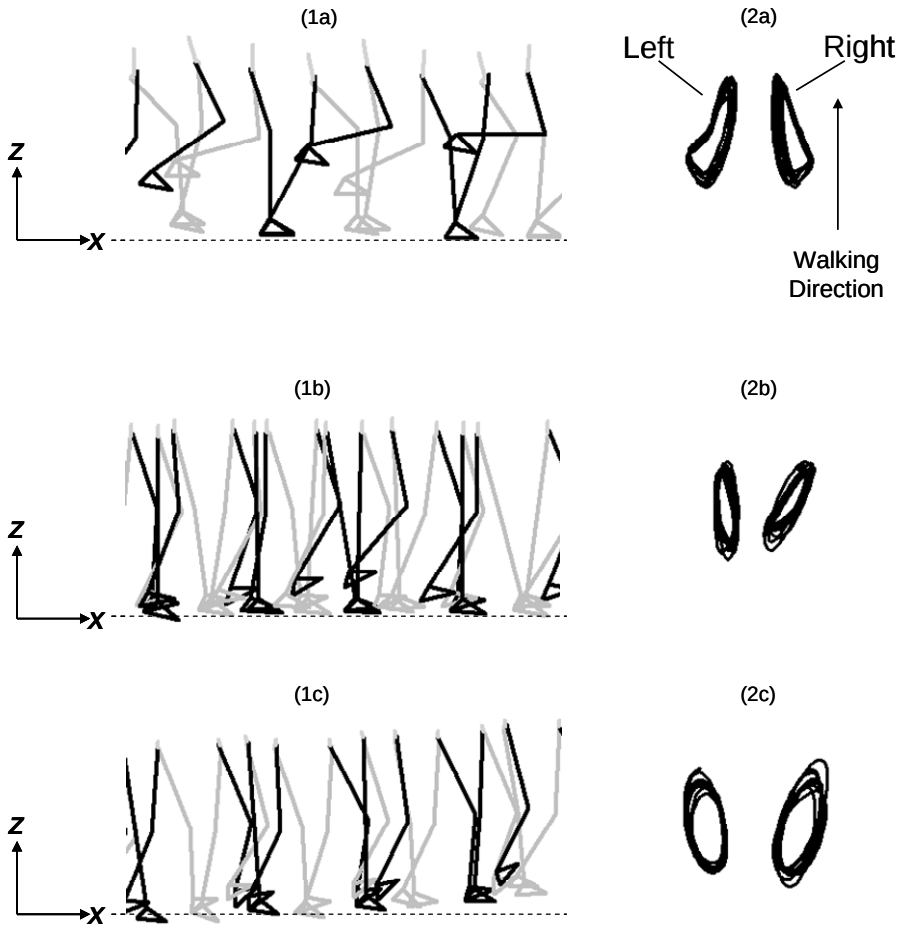

Table1

Gait frequency	a_x^{AB}	a_x^{LT}	a_x^{RT}	a_x^{LS}	a_x^{RS}	a_x^{LF}	a_x^{RF}
Secondary gait frequency (a)	-	16	16	16	16	16	16
Tertiary gait frequency (b)	-	-	-	64	64	64	64
Total (a × b)	-	16	16	1024	1024	1024	1024

(-) : Conditions that are not considered.

Table2

Joint		θ_{min}	θ_{max}
Hip	$\theta_{XZ}^{LT}, \theta_{XZ}^{RT}$	-20 °	90 °
Knee	$\left\|\theta_{XZ}^{LS} - \theta_{XZ}^{LT}\right\|$	0°	120°
	$\left\|\theta_{XZ}^{RS} - \theta_{XZ}^{RT}\right\|$		
Ankle	$\theta_{XZ}^{LF}, \theta_{XZ}^{RF}$	-30° *1	50° *1

0° is the angle of the joint angles during upright standing position.
*1 Plantar flexion and dorsal extension.

Table3

Volunteer	Age	Height (cm)	Primary GF (Hz)	Secondary GF (Hz)	Tertiary GF (Hz)
A (male)	22	180	0.68	1.36	2.00
B (male)	26	173	0.58	1.17	1.80
C (female)	24	155	0.68	1.36	2.05